Effect of Swirl Angle on Interaction between Swirl Oxygen Lance Jet and Melt Pool

Haoran Ma [a], Guangqiang Liu [b,*], Chengcheng Xu [c], Kun Liu [a], Peng Han [a]

[a] College of Materials and Metallurgy, University of Science and Technology Liaoning,
Anshan 3114051, China
[b] College of Civil Engineering, University of Science and Technology Liaoning,
Anshan 114051, China
[c] Cold rolling mill plant, ANGANG Steel Company Limited,
Anshan 114021, China
* Corresponding author: E-mail address: lgqiang0305@sina.com

Abstract

In order to clarify the action law of the swirl oxygen lance jet on the melt pool of the converter and to determine the optimal swirl angle of the swirl oxygen lance for the 120t converter, this study establishes the gas-liquid two-phase flow model of the oxygen lance with different swirl angles based on the realizable k-ε model and the VOF multiphase flow model. The gas-liquid interface behavior during the interaction between the jet and the molten pool was analyzed, and the flow pattern of molten steel in the molten pool was mainly investigated. The results show that compared with traditional oxygen lance, the rotating oxygen lance jet enhances the stirring of the melt pool and intensifies the fluctuation of the melt pool liquid level. The depth of the impact cavity decreases with the increase of the swirl angle, but the diameter of the impact cavity increases with the increase of the swirl angle. When the jet with a swirl angle of 10 ° impacts the surface of the melt pool, the turbulence energy obtained by the molten steel is the highest, the average flow velocity inside the melt pool is the highest, and the molten steel is stirred more thoroughly, achieving better melting effects.

Key words: Swirl oxygen, Melt pool, Swirl angle, Gas-liquid interface, Dead zone.

1. Introduction

The process of converter steelmaking is a complex process involving flow, mass transfer, heat transfer, and physicochemical reactions. At present, the most widely used steelmaking method in the world is the converter top-blowing oxygen steelmaking method [1]. The oxygen lance is a key equipment in the process of converter smelting. During the conventional oxygen lance blowing process, there is a risk of splashing of molten steel outside the furnace, which seriously affects personal safety. Researchers usually use the method of increasing the tilt angle to reduce the occurrence of splashing. However, excessive

inclination angle may cause jet erosion of the furnace lining. Therefore, the structural characteristics of the conventional oxygen lance limit its further development [2]. In order to solve the above problems, researchers further proposed the swirl oxygen lance. Compared with traditional oxygen lance, the oxygen jet of the swirl oxygen lance reduces axial impact force and increases tangential impact force, effectively avoiding premature fusion of the jet, reducing steel splashing, improving slag making effect, and effectively improving blowing efficiency [3]. Wang et al. [4] used Fluent software to simulate the oxygen jet of the rotating oxygen lance and the flow of molten steel in the converter, and found that the rotating oxygen lance nozzle with a

swirl angle of 10 ° had the best effect. Higuchi et al. [5] found through a six hole cold water model experiment that the splashing rate was the lowest when the swirl angle was 11.4°. On the basis of numerical simulation, Li et al. [6] studied the effect of swirl angle on the flow field characteristics of the four hole swirl oxygen lance in a 120t converter, and ultimately chose a swirl angle of 5° after optimization.

It can be seen that there is currently a lack of further exploration and research on the interaction between the swirling oxygen lance, especially the interaction between the rotating oxygen jet and the molten pool. Therefore, this study aims to conduct in-depth research on the interaction between the rotating oxygen lance jet and the melt pool. In order to better demonstrate the action process of the rotating oxygen lance on the converter melt pool, numerical simulation technique based on VOF multiphase flow model was used to simulate the gas-liquid two-phase behavior of the swirl oxygen lance at different swirl angles, and the interaction between the jet and the surface of the melt pool were studied. The interface characteristics of the molten pool under jet impact, changes in surface turbulent kinetic energy, velocity distribution inside the converter, and volume distribution in different areas were analyzed separately.

2. Model building

2.1. Mathematical modelling

The VOF interface tracking technology was adopted to study the gas-liquid two-phase behaviour, and a mathematical model of gas-liquid two-phase flow in a 120t top blown oxygen converter was established. The following four assumptions were made [7]:
1) Oxygen is a compressible fluid, and the molten steel is an incompressible fluid.
2) The fluid flow is a three-dimensional, non-stationary, and non-isothermal process.
3) Neglect the chemical reaction inside the furnace.
4) The physical parameters of the substances in the converter do not change with temperature, i.e., they have constant physical properties.

2.1.1. Basic control equations
During the oxygen converter smelting process, the jet is not only in contact with the ambient medium but also exchanges mass, momentum, and heat with the molten steel. The basic control equations were shown below:
Mass conservation equation:

$$\frac{\partial \rho}{\partial t} + \frac{\partial (\rho u_i)}{\partial x_i} = 0 \tag{1}$$

Conservation of momentum equation:

$$\frac{\partial (\rho u_i)}{\partial t} + \frac{\partial (\rho u_i u_j)}{\partial x_j} = -\frac{\partial p}{\partial x_i} + \frac{\partial (\tau_{ij} - \rho \overline{u_i u_j})}{\partial x_j} \tag{2}$$

The energy conservation equation:

$$\frac{\partial (\rho c_p T)}{\partial t} + \frac{\partial (\rho u_j C_p T)}{\partial x_i} = u_j \frac{\partial P}{\partial x_j} + \tau_{ij} \frac{\partial u_i}{\partial x_j} + \lambda_{eff} \frac{\partial^2 T}{\partial x_j^2} \tag{3}$$

$$\tau_{ij} = \mu_{eff} \left(\frac{\partial u_j}{\partial x_i} + \frac{\partial u_i}{\partial x_j} \right) - \frac{2}{3} \mu_{eff} \frac{\partial u_k}{\partial x_k} \delta_{ij} \tag{4}$$

Where ρ is the oxygen density, kg/m^3; μ is the molecular viscosity, Pa·s; p is the pressure, Pa; τ_{ij} is the viscous stress, Pa; C_p is the specific heat capacity, J/kg·K; λ_{eff} is the effective thermal conductivity, W/m·K; T is the jet temperature, K; u_i is the velocity in the i-direction, m/s; u_j is the velocity in the j-direction, and μ_{eff} is the effective viscosity, Pa·s, and $\mu_{eff} = \mu + \mu_t$.

2.1.2. Multiphase flow model equations
The gas-liquid two-phase fluid in the converter is a continuous medium with mutual permeability. To address the interface problems between different phases, this study chose the VOF multiphase flow model provided by Fluent. Compared with other models, the characteristic of VOF is the introduction of volume fraction α. The phase is regarded as a continuous fluid, and the phase volume fraction α is described as a continuous function of time and space. The volume fraction occupied by each phase in each individual mesh sums to 1, as expressed in the following equation:

$$\sum_{q=1}^{n} \alpha_q = 1 \tag{5}$$

If the volume fraction of the qth phase in a given unit control body is α, there are the following three cases:
1) If $\alpha_q = 1$: the volume cell is considered to have all q-phases.
2) If $\alpha_q = 0$: the volume cell is considered to have no q-phases at all.
3) If $0 < \alpha_q < 1$: the volume cell is considered to have a mixture of q-phases as well as the presence of other phases.

The volume fraction equation and momentum equation in VOF are shown below:
Volume fraction equation:

$$\frac{1}{\rho_q} \left[\frac{\partial (\rho_q \alpha_q)}{\partial t} + \nabla (\alpha_q \rho_q \overrightarrow{u_q}) \right] = 0 \tag{6}$$

Momentum equation:

$$\frac{\partial}{\partial t} (\rho \vec{u}) + \nabla (\rho \vec{u} \vec{u}) = -\nabla p + \nabla \cdot \left[\mu_{eff} \left(\nabla \vec{u} + \nabla \vec{u}^T \right) \right] + \rho \vec{g} + f_\sigma \tag{7}$$

ρ_q and α_q are the density and volume fraction of phase q, respectively. For oxygen, the ideal gas law is satisfied, that is, $p = \rho RT$. μ_{eff} is the effective viscosity, Pa·s; f_σ is the surface tension, N/m^3; $\vec{u}$ is the velocity vector, m/s; $\vec{g}$ is the acceleration vector of gravity, m/s^2.

2.1.3. Turbulence model equation

The realizable *k-ε* model was used to study the gas-liquid phase of the oxygen lance and melt pool. The transport equations for turbulent kinetic energy k and turbulent dissipation rate ε are:

$$\frac{\partial(\rho k)}{\partial t} + \frac{\partial(\rho k u_i)}{\partial x_i} = \frac{\partial}{\partial x_j}\left[\left(\mu + \frac{\mu_t}{\sigma_k}\right)\frac{\partial k}{\partial x_j}\right] + G_k + G_b - \rho\varepsilon - Y_M + S_k \quad (8)$$

$$\frac{\partial(\rho\varepsilon)}{\partial t} + \frac{\partial(\rho\varepsilon u_i)}{\partial x_i} = \frac{\partial}{\partial x_j}\left[\left(\mu + \frac{\mu_t}{\sigma_\varepsilon}\right)\frac{\partial\varepsilon}{\partial x_j}\right] + \rho C_1 S_\varepsilon - \rho C_2 \frac{\varepsilon^2}{k+\sqrt{v\varepsilon}} + C_{1\varepsilon}\frac{\varepsilon}{k}C_{3\varepsilon}G_b + S_\varepsilon \quad (9)$$

where, G_k is the turbulent energy generation term caused by the gradient of average velocity, kg/m·s³; G_b is the generation term of turbulent energy k caused by buoyancy, kg/m·s³; Y_M is the effect of pulsation expansion on the total dissipation rate in compressible turbulence. σ_k is the Prandtl number corresponding to turbulent kinetic energy k. σ_ε is the Prandtl number corresponding to the dissipation rate ε. S_k and S_ε are user-defined source items. Empirical constants $C_{1\varepsilon}$=1.44, C_2=1.9, σ_k=1.0, σ_ε=1.2.

2.2. Physical model establishment

2.2.1. Determination of model size and parameters

A three-dimensional model of the 120t converter in a steel plant was established as the research object. Based on the oxygen lance with an inclination angle of 14°, the influence of the oxygen lance with different swirl angles on the smelting process of the converter is analyzed. The structural parameters of the converter and the oxygen lance are shown in Table 1.

Table 1.
Structural parameters of converter and lance

Structure of converter and oxygen lance	Argument
Melt pool radius, R/ mm	2580
Bottom radius, r/ mm	1568
Melt pool depth, h / mm	1244.4
Inlet diameter, d_e/ mm	47.4
Oxygen lance height, H/ m	1.68
Inclination angle, α/°	14
Swirl angle, β/°	0/5/8/10/13

2.2.2. Geometric modelling and boundary condition determination

The geometric model is established using Solidworks software, and part of the converter body is selected as the calculation domain. In order to facilitate the calculation and improve the calculation efficiency while ensuring the calculation accuracy, a five-hole swirl oxygen lance is selected, and 1/5 of the whole furnace body is selected for calculation in this research, and the schematic diagram of the physical model is shown in figure 1(a). Gambit is used for grid partitioning, and hexahedral grids are adopted to adapt to the gas-liquid interface motion that captures significant changes in velocity and temperature gradients during the research process. The area near the nozzle outlet and the gas-liquid interface were encrypted [8]. Figure 1(b) below shows the schematic diagram of the grid division.

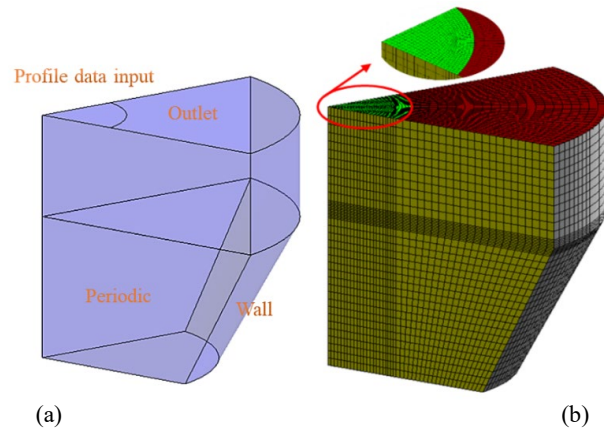<center>(a)   (b)</center>

Fig. 1. Schematic diagram of physical model

The ANSYS fluid dynamics software was used for the analysis and unsteady state process. The boundary conditions were set as shown in Table 2.

The numerical study by Muñoz-Esparza [9] on the influence of gas jet on deformable liquid layers shows that the standard k-ω and standard k-ε models may lead to negative strain when the strain rate of the time average velocity is particularly high. Therefore, this study chose the realizable k-ε model to increase the constraint of Reynolds stress, making it consistent with real turbulence to simulate the diffusion velocity of flat and cylindrical jets more accurately.

Based on the multi-phase flow boundary condition setting methods of Zhou [10] and Hu[11], this study first intercepts the cross-section of the jet with different lance positions at a temperature of 1873K under the realizable k-ε turbulence model and then extracts the velocity values in the x, y, and z directions of this cross-section. The values of static water pressure, turbulent kinetic energy, and turbulent dissipation rate are input into the two-phase flow model as inlet boundary conditions The outlet is set as a pressure outlet. The spatial interface inside the converter was calculated using periodic boundary conditions. A pressure-based solver was used to calculate the flow field, and the PISO algorithm was used to calculate the pressure-velocity coupling. The PRESTO discrete format was used to calculate the interpolation of the pressure, and the CICSAM format was used to calculate the interpolation of the free interface. The second-order differential headwind format was used to compute the discretization of turbulent kinetic energy and turbulent dissipation rate [12]. The initial time step was set as 10⁻⁴, and its dynamic criterion was subsequently set to adaptive, which automatically adjusts the time step computation time when the Courant number is less than 1. The computation is considered convergent when the residuals of the energy are less than 10⁻⁶ and the residuals of the other variables are less than 10⁻³[13]. Table 3 shows the fluid physical property parameters set in this simulation.

Table 2.
Boundary condition parameters

Boundary condition	Argument
Furnace pressure, P_b/ MPa	0.104
Furnace temperature, T_b/ K	1873

Table 3．
Physical properties of fluids

Physical properties of fluids	Molten steel	Oxidation
Density, ρ/ kg/m³	7000	-
Viscosity, μ/ Pa.s	0.0065	$1.19×10^{-5}$
Surface tension, σ/N/m	1.6	-
Heat capacity, C_P/ J/ kg.k	670	919.31
Thermal conductivity, λ/W/m.	40	0.0246
Temperature, T/ k	1873	-

2.2.3. Grid independence test

In this thesis, the grid independence test was carried out on the model applied in the simulation research of the interaction between swirl oxygen lance jet and the melt pool.

The grid number scheme (A, B, C, D) was calculated, with grid numbers of 1,100,000, 850,000, 600,000 and 350,000 respectively. The simulation calculation of the four schemes is carried out under the condition that other settings are the same. The velocity distribution of the center line of the different number of mesh jets is shown in Figure 2, where R is the distance between the center of the jet and the axis of the oxygen lance nozzle. The results show that the difference in calculation results between A and B is the smallest, but Scheme A has 1.1 million grids, which is 250000 more than Scheme B. Considering the impact of simulation accuracy and calculation cost, this thesis finally selects Scheme B, and the number of grids selected is about 850,000.
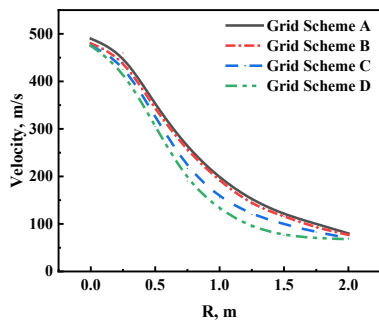

Fig. 2. Distribution of center line velocity of different number of mesh jets

2.2.4. Turbulence model validation

The turbulence model verification in this thesis is based on Chao F [14]. In the thesis of Chao F, the Mach number is 2.04, the nozzle throat diameter of the oxygen lance is 37.4mm, the outlet diameter is 49.4mm, the main nozzle angle is 13°, the swirl angle is 10°, and the expansion section half-guide angle is 4° to establish a four hole swirl oxygen lance model. The conditions set are the same as the numerical simulation set in this thesis, and the numerical simulation operation is carried out in the realizable k-ε turbulence model. The simulation result distribution of axial jet velocity of the nozzle is drawn as Figure 3, and the comparison with the jet test results in this thesis shows that, the difference between the simulation results of realizable k-ε turbulence model and the experimental results is very small, which proves that the turbulence model in this thesis is reasonable to choose realizable k-ε turbulence model.
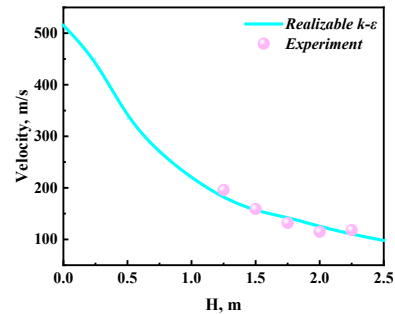

Fig. 3. Comparison of turbulence model simulation data and experiment

3. Analysis and discussion of the results

3.1. Gas-liquid interface characteristics in the converter

Under the impact of porous oxygen jet, several small and deep cavities or single large and shallow cavity will form on the surface of the melt pool. The shape of the impact cavity affects the early slagging and subsequent decarbonization effects and has a significant impact on converter smelting. The swirl angle has a significant impact on the width and depth of the impact pit, which has a significant impact on the entire smelting process. Therefore, studying the depth and width of the gas-liquid interface impact pit in the melt pool under different swirl angles can provide guidance for the selection of swirl angle of the swirl oxygen lance in industrial production.

Figure 4 shows the surface morphology distribution of the melt pool when oxygen lances with different swirl angles corresponding to the inclination angle of 14° are blown to 12.5s at $H=35de$ position. It can be seen from the figure that the impact cavity formed by the swirl oxygen lance on the gas-liquid interface of the melt pool is significantly less deep than that of the traditional oxygen lance, but the width is significantly larger than that of the traditional oxygen lance, and this law becomes more and more obvious with the increase of the swirl angle. This is because the swirl angle causes the jet to generate tangential velocity, which increases with the increase of the swirl angle. The width of the impact cavity will increase with the increase of tangential velocity, but the depth of the impact cavity will become shallower with the increase of tangential velocity [15]. Figure 5

shows a schematic diagram of the cavity shape. The width is defined as the maximum diameter distance of the impact cavity, and the depth is defined as the maximum depth of the impact cavity relative to the surface of the molten pool. Figure 6 shows the width and depth of the impact cavity formed by the impact of oxygen lance jet with different swirl angles on the molten pool. The results in figure 6 further indicate that as the swirl angle increases, the depth of the impact cavity decreases, but the width of the impact cavity increases. This result is consistent with relevant research findings [16].
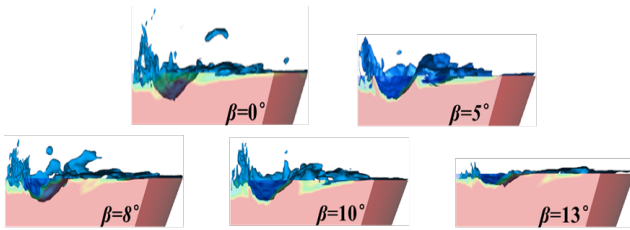
Fig. 4. Surface morphology distribution of oxygen lances with different swirl angles at 35de lance level
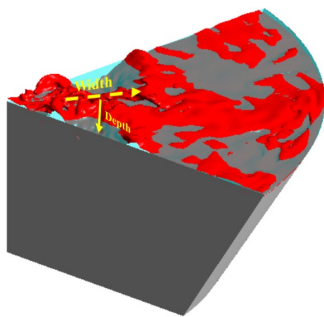
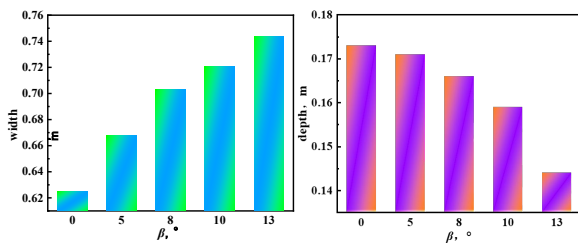Fig. 5. Diagram of width and depth of impact crater

Fig. 6. Width and depth of impact crater comparison

The turbulent kinetic energy distribution when the oxygen lance jet reaches the surface of the molten steel is an important indicator to measure the blowing effect of the oxygen lance. Figure 7 is the cloud diagram of turbulent kinetic energy distribution on the melt pool surface when the vortex angle of 14° inclination is blown to 12.5s at $H=35de$. It can be observed that compared to traditional oxygen jets, the turbulent kinetic energy on the surface of the molten steel is greater when the swirling oxygen lance jet impacts the molten pool. This is because the existence of the vortex angle provides a certain tangential velocity for the jet. Tangential velocity increases the stirring effect of the jet stream on the melt pool, so that the turbulent kinetic energy at the liquid surface is larger than that of the traditional oxygen

lance. This conclusion can be more directly seen from the quantified turbulent kinetic energy shown in Figure 8, where it can be observed that the turbulent kinetic energy initially increases with the increase of swirl angle. This is because with the increase in the swirl angle, the tangential velocity of the jet increases gradually, stirring the melt pool more fully and thus increasing the turbulent kinetic energy. The turbulent kinetic energy reaches its peak value at a swirl angle of 10°. However, when the swirl angle increases to 13 °, although the tangential velocity increases the impact range of the jet, the impact amplitude of the jet will still expand due to the large swirl angle. The rapid overall velocity attenuation results in a large decrease in the impact depth, and then the turbulent kinetic energy decreases with the continuous increase of the swirl angle.
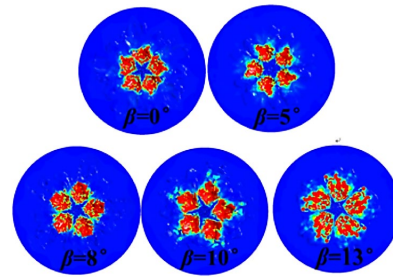

Fig. 7. Distribution of turbulent kinetic energy on melt pool surface at 35de lance level for oxygen lances with different swirling angles
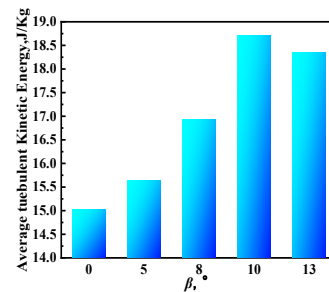

Fig. 8. Comparison of turbulent kinetic energy on melt pool surface

3.2. Velocity distribution in the converter cross-section

Figure 9 shows the velocity distribution cloud diagram of the cross section of the oxygen lance with different swirl angles at the angle of 14° for blowing time 3s at the depth of 0.1m melt pool. The velocity distribution near the center area of the melt pool in this section is relatively large, because the melt pool fluid is drawn by various jets and gathers in this area to obtain large kinetic energy. The area with large velocity value here is defined as the jet impact area. It can be basically determined that the velocity of the jet impact area is about 0.2m/s by observing the velocity cloud map of the cross section. It can also be seen from the figure that the velocity of melt pool cross section gradually

increases with the increase of swirl angle. Figure 10 compares the average velocity values of the cross-section under different swirl angles when the depth of the melt pool is 0.1m. It can be seen more intuitively that the circulating velocity inside molten steel of swirl oxygen lance with different swirl angle is higher than that of traditional oxygen lance.

As the swirl angle increases, the average velocity first increases and then decreases, and the maximum average velocity is achieved at a swirl angle of 10 °. This is because as the swirl angle increases, the flow velocity of molten steel increases. When the swirl angle increases to a certain extent, if it continues to increase, the tangential velocity component is too large, which reduces the axial impact ability of the jet stream and weakens the impact effect on the melt pool. Molten steel only undergoes agitation at the surface of the melt pool due to the effect of tangential velocity [17]. As the depth of the melt pool increases, the axial impact force of the jet weakens, and the axial impact force has little effect on the melt pool and will not cause more intense stirring. This is manifested as the average velocity value of the entire cross-section not increasing but decreasing [18]. When using a 10 ° swirl oxygen lance nozzle for spraying, the flow rate of molten steel in the melt pool is the highest, indicating that the 10 ° swirl angle has the best stirring effect on the melt pool, improving the production efficiency of steel and making it easier to achieve the best smelting effect during the converter smelting process.
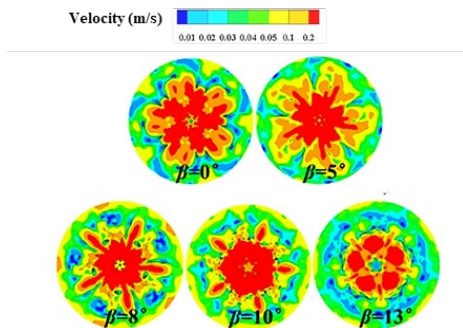

Fig. 9. different swirl angle of oxygen lance under 35de lance level a melt pool depth of 0.1 m the cross section of the velocity distribution
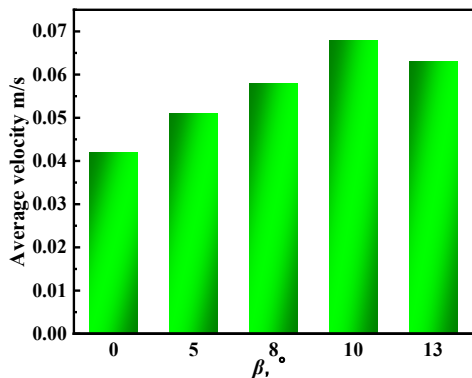

Fig. 10. Average velocity of different swirl angles at a cross-section with a depth of 0.1m

3.3. Velocity distribution at different radial distances in the converter

Figure 11 shows the three-dimensional velocity distributions of three different oxygen lances at different radial distances for 0°, 8°, and 13° swirl angles, with a blowing time of 12.5 s. The velocity of the oxygen lance decreases with the increase of radial distance, because the jet stream impacts the surface of the melt pool and forms pits due to the impact force. The liquid near the pits in the melt pool gains a greater velocity under the impact force and flows outward. However, as the radial distance increases, the flow rate will rapidly decay after mixing with other external liquid parts. It can also be seen from the figure that the liquid velocity inside the melt pool at any radial distance decreases sharply with the increase in depth of the melt pool. Near the gas-liquid two-phase junction, the velocity inside the melt pool is about 0.1 m/s; near the bottom of the melt pool, the velocity has been reduced to 0.03 m/s or so, a decrease of about 70%.

When the inclination angle is constant, an increase in the swirl angle will increase the radial velocity. This is because under the same conditions, when traditional oxygen lance nozzles blow, the surface fluctuation of the molten steel outside the center pit is relatively small, making it difficult to drive the fluctuation inside the melt pool together. However, due to the presence of swirl angle, the contact area between the jet and the melt pool is larger than that of traditional oxygen lance. The surface fluctuation amplitude and range of molten steel in the melt pool are relatively large, and the almost entire surface fluctuation of molten steel extends inward to the inside of the molten steel, making the flow in the melt pool more intense. The larger the swirl angle, the larger the contact area between the jet and the surface of the molten steel, thereby increasing the stirring of the jet outside and at the bottom of the melt pool, providing good dynamic conditions for the melt pool reaction, which is conducive to the rapid and efficient progress of the melt pool reaction. Therefore, the swirl oxygen lance nozzle can better promote the flow of fluid in the melt pool, making the melt pool quickly become uniform.
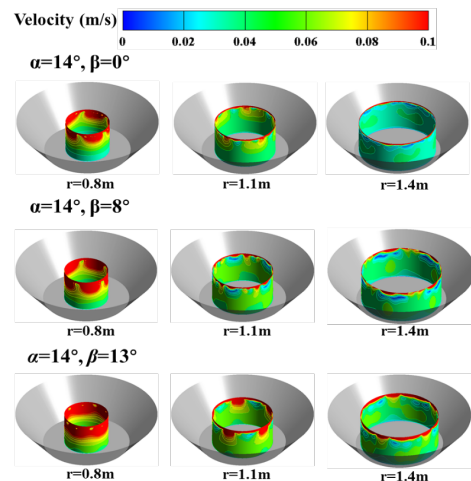

Fig. 11. Velocity distribution at different radial distances in the melt pool

Figure 12 compares the average velocity of different radial sections in the melt pool, and it can be seen that the larger the radial distance of the same oxygen lance, the smaller the average velocity. When the inclination angle is 14 °, as the swirl angle increases, the average velocity of the melt pool shows a trend of first increasing and then decreasing, reaching its peak at a swirl angle of 10 °. The maximum average speed value is 0.072m/s. When the swirl angle increases from 10 ° to 13 °, the flow rate of molten steel in the melt pool does not increase, which is consistent with the number of swirl angles corresponding to the peak velocity distribution of oxygen lance with different swirl angles mentioned earlier. Therefore, a swirl angle of 10 °for the 120t converter swirl lance is the optimal angle, which can effectively stir the melt pool and achieve good smelting effect in the converter smelting process.
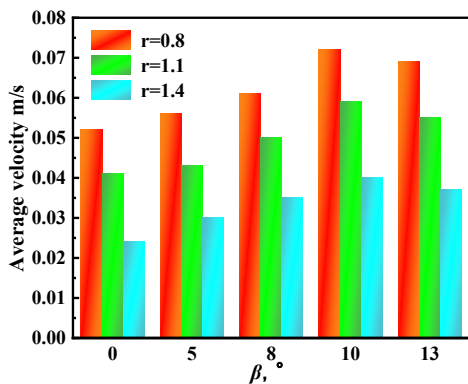

Fig. 12. Average velocity of different radial sections in melt pool

3.1. Volume distribution in different areas of the melt pool

Figure 13 shows the velocity distribution in the melt pool during 2.5 seconds of oxygen lance blowing with different swirl angles. The area where the velocity of the molten steel in the melt pool is greater than 0.1m/s is defined as the high-speed zone, the area where the velocity is between 0.03m/s and 0.1m/s is the weak stirring zone, and the area where the velocity is below 0.03m/s is the dead zone. The influence of changes in swirl angle on the volume distribution of different regions inside the melt pool was investigated based on the area of these three regions. The area of these three zones is taken as the object of study to investigate the effect of the variation of the swirl angle on the volume distribution of different regions inside the melt pool.

It can be observed that the high-speed zone is concentrated near the impact pits formed by the oxygen jet impacting the melt pool. This is because the oxygen jet stream impacts the surface of the molten steel, resulting in a higher flow velocity of the molten steel in that area. But the energy possessed by the jet is not sufficient to allow it to penetrate the entire interior of the melt pool. After the impact of the jet on the melt pool forms an impact cavity, the molten steel with higher flow velocity diffuses around and mixes with the relatively stationary molten steel around it [19]. When the mixed molten steel with a certain flow rate reaches the area where the surface of the melt pool comes into contact with the furnace wall, it is hindered by the furnace wall and the flow rate of the molten steel suddenly decreases, below 0.03m/s. So there is a large volume distribution of dead zones in the area where the surface of the melt pool contacts the furnace wall. The velocity of the molten steel gradually decreases, and when it reaches the bottom of the melt pool, the velocity value is too small, forming a dead zone [20]. The rest of the velocity ranges from 0.003 to 0.1m/s, which is a weak stirring zone.
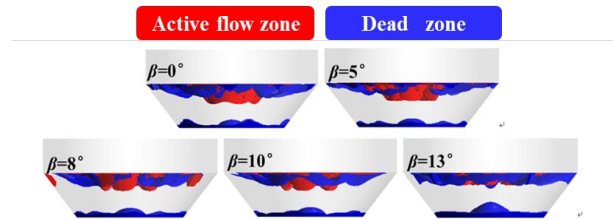

Fig. 13. Volume distribution of different regions in the melt pool

Figure 14 shows the volume fraction ratios of different regions in the oxygen gun melt pool at different swirl angles. As the swirl angle increases, the tangential velocity of the jet increases, and the ability of the melt pool to rotate horizontally increases. This means that the stirring of the jet on the melt pool is strengthened, and the flow rate of molten steel in the pool increases. Therefore, the volume ratio in the high-speed area gradually increases. When the swirl angle is 10 °, the high-speed zone reaches its maximum value. When the swirl angle increases to 13 °, the tangential component of the oxygen lance jet increases. This leads to a decrease in the axial impact ability of the jet, a decrease in the flow rate of the molten steel, a decrease in the proportion of high-speed zone volume in the melt pool, and an increase in the proportion of dead zone volume.
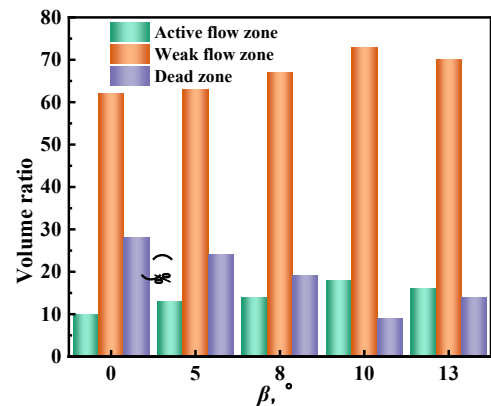

Fig. 14. Volume fraction ratio of different regions in the melt pool

4. Conclusions

1) Compared with traditional oxygen lance, the swirling oxygen lance enhances the stirring of the melt bath and exacerbates the fluctuation of the molten steel.
2) As the swirl angle increases, the depth of the impact crater decreases, and the diameter of the impact crater increases.

3) As the swirl angle increases, the tangential velocity of the jet increases, and the rotational motion of the melt bath is enhanced. Excessive swirl angle leads to excessive tangential force of the jet, thereby weakening the axial impact capacity.

4) When the jet with a swirl angle of 10° impacts the surface of the melt pool, the turbulence energy obtained by the molten steel is the highest, the average flow velocity inside the melt pool is the highest, and the molten steel is stirred more thoroughly, achieving better melting effects.

Acknowledgment

References

[1] Rao, J.P., Li, G.Q., & Yang, Z.Z. (2011). Research and application of new oxygen lance for BOF steelmaking. *Advanced Materials Research.* 335, 74-79. https://doi.org/10.4028/www.scientific.net/AMR.335-336.74.

[2] Allemand, B., Bruchet P. & Champinot, C. (2001). Theoretical and experimental study of supersonic oxygen jets. Industrial application in EAF. *Metallurgical Research & Technology.* 98(6), 571-587. https://doi.org/10.1051/metal:2001107.

[3] Li, L., Li, M. & Shao, L. (2020). Physical and mathematical modeling of swirling gas jets impinging onto a liquid bath using a novel nozzles-twisted lance. *Steel Research International.* 91(7), 54-60. https://doi.org/10.1002/srin.201900684.

[4] Wang, X. (2022). *Numerical simulation of jet characteristics and gas liquid two phase behavior of swirling oxygen lance.* University of Science and Technology Liaoning. https://doi.org/10.26923/d.cnki.gasgc.2021.000081.

[5] Higuchi, Y. & Tago, Y. (2003). Effect of nozzle twisted lance on jet behavior and spitting rate in top blown process. *ISIJ international.* 43(9), 1410-1414. https://doi.org/10.2355/isijinternational.43.1410.

[6] Li, M., Li, Q. & Kuang, S. (2016). Computational investigation of the splashing phenomenon induced by the impingement of multiple supersonic jets onto a molten slag–metal melt pool. *Industrial & Engineering Chemistry Research.* 55(12), 3630-3640. https://doi.org/10.1021/acs.iecr.5b03301.

[7] Li, Q., Li, M. & Kuang, S, B. (2014). Computational study on the behaviours of supersonic jets and their impingement onto molten liquid free surface in BOF steelmaking. *Canadian Metallurgical Quarterly.* 53(3), 340-351. https://doi.org/10.1179/1879139514Y.0000000124.

[8] Li, M., Li, Q. & Zou Z. (2017). Computational investigation of swirling supersonic jets generated through a nozzle-twisted lance. *Metallurgical and Materials Transactions B.* 48, 713-725. https://doi.org/10.1007/s11663-016-0851-2.

[9] Muñoz-Esparza, D., Buchlin, J.M. & Myrillas, K. (2012). Numerical investigation of impinging gas jets onto deformable liquid layers. *Applied Mathematical Modelling.* 36(6), 2687-2700. https://doi.org/10.1016/j.apm.2011.09.052.

[10] Zhou, X., Ersson, M. & Zhong, L. (2014). Mathematical and physical simulation of a top blown converter. *Steel research international.* 85(2), 273-281. https://doi.org/10.1002/srin.201300310.

[11] Hu, S., Zhu, R., & Dong, K. (2018). Effect of oxygen flow rate and temperature on supersonic jet characteristics and fluid flow in an EAF molten bath. *Canadian Metallurgical Quarterly.* 57(2), 219-234. https://doi.org/10.1080/00084433.2017.1409945.

[12] Wang, W., Yuan, Z., & Matsuura, H. (2010). Three-dimensional compressible flow simulation of top-blown multiple jets in converter. *ISIJ International.* 50(4), 491-500. https://doi.org/10.2355/isijinternational.50.491.

[13] Li, M., Li, L. & Zhang, B. (2020). Numerical analysis of the particle-induced effect on gas flow in a supersonic powder-laden oxygen jet. *Metallurgical and Materials Transactions B.* 51, 1718-1730. https://doi.org/10.1007/s11663-020-01855-3.

[14] Feng, C., Zhu, R. & Dong, K. (2021). Effects of ambient temperature and powder gas ratio on jet characteristics of O2+ CO2 and CaO particles injected by a swirl-type oxygen lance nozzle. *Powder Technology.* 388, 537-553. https://doi.org/10.1016/j.powtec.2021.04.085.

[15] Lv, M., Zhu, R. & Wang H. (2013). Simulation and application of swirl-type oxygen lance in vanadium extraction converter. *Steel Research International.* 84(3), 304-312. https://doi.org/10.1002/srin.201200136.

[16] Lv, M., Zhu, R. & Guo, Y.G. (2013). Simulation of flowfluid in the BOF steelmaking process. *Metallurgical and Materials Transactions B.* 44, 1560-1571. https://doi.org/10.1007/s11663-013-9935-4.

[17] Alam, M., Naser, J., & Brooks, G. (2010). Computational fluid dynamics simulation of supersonic oxygen jet behavior at steelmaking temperature. *Metallurgical and Materials Transactions B.* 41, 636-645. https://doi.org/10.1007/s11663-010-9341-0.

[18] Liu, F., Sun, D. & Zhu, R. (2017). Effect of nozzle twisted oxygen lance on flow field and dephosphorization rate in converter steelmaking process. *Ironmaking & Steelmaking.* 44(9), 640-648. https://doi.org/10.1080/03019233.2016.1226562.

[19] Zhong, L., Zhu, Y. & Jiang, M. (2005). Cold modelling of slag splashing in LD furnace by oxygen lance with twisted nozzle tip. *Steel Research International.* 76(9), 611-615. https://doi.org/10.1002/srin.200506065.

[20] Liu, G., Liu, K., & Han, P. (2021). Splash sheet characteristics induced by the impingement of multiple jets in a steelmaking converter. *Ironmaking & Steelmaking.* 48(1), 25-32. https://doi.org/10.1080/03019233.2020.1720453.